

SMAT: Staged Multi-Agent Training for Co-Adaptive Exoskeleton Control

Yifei Yuan, Ghaith Androwis, and Xianlian Zhou

Abstract—Effective exoskeleton assistance requires co-adaptation: as the device alters joint dynamics, the user reorganizes neuromuscular coordination, creating a non-stationary learning problem. Most learning-based approaches do not explicitly account for the sequential nature of human motor adaptation, leading to training instability and poorly timed assistance. We propose Staged Multi-Agent Training (SMAT), a four-stage curriculum designed to mirror how users naturally acclimate to a wearable device. In SMAT, a musculoskeletal human actor and a bilateral hip exoskeleton actor are trained progressively: the human first learns unassisted gait, then adapts to the added device mass; the exoskeleton subsequently learns a positive assistance pattern against a stabilized human policy, and finally both agents co-adapt with full torque capacity and bidirectional feedback. We implement SMAT in the MyoAssist simulation environment using a 26-muscle lower-limb model and an attached hip exoskeleton. Our musculoskeletal simulations demonstrate that the learned exoskeleton control policy produces an average 10.1% reduction in hip muscle activation relative to the no-assist condition. We validated the learned controller in an offline setting using open-source gait data, then deployed it to a physical hip exoskeleton for treadmill experiments with five subjects. The resulting policy delivers consistent assistance and predominantly positive mechanical power without the need for any explicitly imposed timing shift (mean positive power: 13.6 W at 6 Nm RMS torque to 23.8 W at 9.3 Nm RMS torque, with minimal negative power) consistently across all subjects without subject-specific retraining.

I. INTRODUCTION

Lower-limb exoskeletons offer a promising avenue for gait rehabilitation and physical augmentation, but effective assistance requires controllers that can adapt to the unique biomechanics of each user [1], [2]. In practice, this is a co-adaptation problem: as the device adjusts assistance, the user simultaneously reorganizes neuromuscular coordination, altering joint kinematics, muscle activations, and inter-limb timing [3]. The result is a tightly coupled human–device system in which both agents influence each other.

Recent advances in AI and reinforcement learning (RL) have enabled data-driven optimization of exoskeleton control policies in simulation. Musculoskeletal simulation combined with RL has demonstrated robust policy learning for exoskeleton control [4], and joint human-exoskeleton training with sim-to-real transfer has been demonstrated for walking and related activities [5]. Subsequent studies extended simulation-based RL to broader assistance scenarios, including human-aligned frameworks that predict adaptation

across walking speeds [6], ankle assistance for gait asymmetry [7], and multi-joint squatting tasks [8]. Yet none of these approaches explicitly accounts for how human motor coordination evolves as users acclimate to the device.

Despite these advances, a fundamental challenge remains unresolved: the learning problem is inherently non-stationary. As the exoskeleton policy improves, the human policy simultaneously adapts, altering the underlying state distribution. Without structured coordination, jointly optimizing both agents can lead to instability, including oscillatory torque outputs, poorly timed assistance, and destabilized training dynamics. Existing approaches typically address reward design or policy robustness, but they do not explicitly model or structure the sequential nature of human motor adaptation during device acclimation.

Prior work on musculoskeletal skill learning suggests that curriculum-based reinforcement learning can improve training stability and the physiological plausibility of learned motor policies [9], [10], [11]. Analogously, human users often need to stabilize gait coordination before they can reliably benefit from active assistance. These observations motivate a structured training protocol that treats motor adaptation as a staged process, which progressively introduces the device load and assistance as the human policy stabilizes.

To address this gap, we present **SMAT** (Staged Multi-Agent Training), a structured curriculum learning protocol for co-adaptive hip exoskeleton control. SMAT trains two control policies (human policy π_h and exoskeleton policy π_e) through four stages: (1) baseline gait learning, (2) adaptation to the attached exoskeleton mass, (3) exoskeleton assistance pattern learning with a frozen human policy, and (4) final human-exoskeleton co-adaptation. By progressively introducing device load and assistance while stabilizing the human policy, SMAT reduces non-stationarity and improves training robustness.

We implement SMAT in the open source MyoAssist simulation environment [12] using a 26-muscle lower-limb model. The learned controller is evaluated using open-source gait data and online treadmill experiments with five human subjects. The main contributions of this work are: (1) a staged multi-agent training framework for co-adaptive hip exoskeleton control that improves training robustness through stage-wise reward decomposition, (2) a modular four-stage training pipeline that separates human adaptation and assistance learning and can generalize to other assistive devices, (3) simulation and hardware validation demonstrating reduced hip muscle activation, smooth and stable torque profiles, and potent assistive power across subjects; and (4)

Yifei Yuan and Xianlian Zhou are with the Department of Biomedical Engineering, New Jersey Institute of Technology, Newark, NJ 07102, USA (yy72@njit.edu, alexzhou@njit.edu). Ghaith Androwis (GAndrowis@kesslerfoundation.org) is with Kessler Foundation, West Orange, NJ, 07052, USA

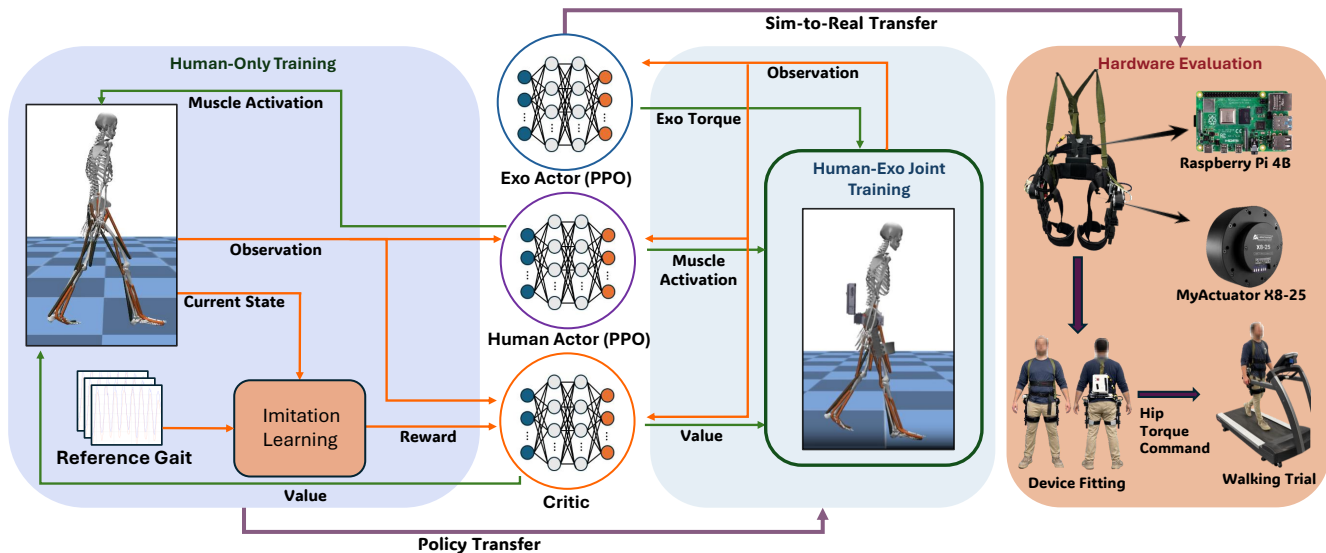


Fig. 1. Overview of the SMAT framework. Two PPO-based actors, a musculoskeletal human actor π_h and an exoskeleton actor π_e , interact with a shared physics simulation through a shared critic V_ψ . *Human-Only Training* (left): only π_h updates via imitation learning from a reference gait. *Human-Exo Joint Training* (center): both actors train simultaneously. *Hardware Evaluation* (right): the trained exoskeleton policy is deployed via sim-to-real transfer, running on a Raspberry Pi 4B to command bilateral MyActuator X8-25 actuators during treadmill walking trials. In SMAT, Stage 1 resides in the human only training mode; Stage 2 adapts the human actor with added exoskeleton mass; Stage 3 freezes the human actor and only trains the exo actor for positive assistance timing; and finally Stage 4 trains both actors for co-adaptation. Policies trained in each stage are subsequently transferred to the next stage.

an ablation analysis of training instabilities in co-adaptive RL for assistive devices. The code will be made publicly available upon acceptance.

II. METHOD

A. Multi-Agent Reinforcement Learning Framework

We formulate hip exoskeleton assistance as a multi-agent reinforcement learning (MARL) problem [5], [12] and implement it within a configurable actor-critic framework. As illustrated in Fig. 1, the framework includes two learning agents, a human actor π_h and an exoskeleton actor π_e , operating in a shared physics simulation that couples a musculoskeletal human model with an exoskeleton.

The human actor receives a musculoskeletal body-state observation and directly outputs 26 muscle activations $\mathbf{a} \in [0, 1]^{26}$ (13 per side), implemented as an MLP with hidden sizes [256, 128]. The policy directly controls muscle excitations, allowing emergent gait patterns to arise from neuromuscular dynamics. The exoskeleton actor receives an 18-dimensional observation \mathbf{o}_e consisting of a three-step history of bilateral hip flexion angles and angular velocities (12 dimensions, 4 dims per timestep) together with a three-step history of its own action (normalized torque) outputs $[\hat{u}_r, \hat{u}_l]$ (6 dimensions, 2 dims per timestep). The exoskeleton actor outputs normalized bilateral hip torque commands $\hat{\mathbf{u}} \in [-1, 1]^2$, which are scaled by stage-dependent torque limits to produce physical assistance, implemented as an MLP with hidden sizes [128, 64]. Both actors share a critic with hidden sizes [256, 128].

TABLE I

STAGE-WISE REWARD CONFIGURATION AND WEIGHTS USED IN THE MULTI-STAGE CURRICULUM.

Reward term	Stage 1	Stage 2	Stage 3	Stage 4
r_{fwd}	0.8	0.8	1.5	1.5
r_{muscle}	0.01	0.01	0.15	0.15
$r_{\Delta a}$	0.005	0.005	0.05	0.05
$r_{\text{hip-act}}$	—	—	2.0	5.0
r_{exo}	—	—	4.0	4.0
$r_{\Delta \tau}$	—	—	—	1.0
Imitation ($r_{\text{qpos/qvel}}$)	1.0	1.0	1.0*	1.0*
$r_{\text{constraint}}$	—	—	0.5	0.5
r_{foot}	—	—	0.3	0.3

* Hip flexion imitation weights are set to zero in Stages 3 and 4 while other joint imitation terms remain active. — indicates that the term is inactive in that stage. In this table, r_{exo} denotes the Stage 3 exoskeleton reward in Eq. (4) and the Stage 4 exoskeleton reward in Eq. (5).

B. Multi-stage Curriculum Training

To mitigate non-stationarity in co-adaptive learning, we decompose training into four stages. Each stage isolates a specific adaptation challenge, progressively introducing mechanical coupling and active assistance. Algorithm 1 summarizes the training schedule, policy freezing, and reward activation.

The stages are designed to sequentially address: (1) Stable human gait generation, (2) Adaptation to exoskeleton mass and inertia, (3) Learning assistance timing, (4) Full human–exoskeleton co-adaptation. This structured progression prevents simultaneous optimization of all objectives, improving stability and convergence.

Stage 1 (Human Baseline Gait Learning). Stage 1 trains a human-only locomotion policy without the exoskeleton.

The goal is to obtain a stable walking policy that mimics a reference gait and serves as the baseline for later stages. The per-timestep reward, with imitation terms adopted from [12], is

$$r^{(1)} = w_{\text{fwd}} r_{\text{fwd}} + w_{\text{mus}} r_{\text{muscle}} + w_{\text{qpos}} r_{\text{qpos}} + w_{\text{qvel}} r_{\text{qvel}} + w_{\Delta a} r_{\Delta a}, \quad (1)$$

where

$$r_{\text{fwd}} = \Delta t \cdot \exp(-5(v - v^*)^2), \quad (2a)$$

$$r_{\text{muscle}} = -\frac{\Delta t}{N_m} \sum_{j=1}^{N_m} a_j, \quad (2b)$$

$$r_{\text{qpos}} = \Delta t \sum_{i \in \mathcal{J}} w_i \exp(-8(q_i - q_i^{\text{ref}})^2), \quad (2c)$$

$$r_{\text{qvel}} = \Delta t \sum_{i \in \mathcal{J}} w_i \exp(-8(\dot{q}_i - \rho \dot{q}_i^{\text{ref}})^2), \quad (2d)$$

$$r_{\Delta a} = \frac{\Delta t}{N_m} \sum_{j=1}^{N_m} \exp(-4(a_{j,t} - a_{j,t-1})^2). \quad (2e)$$

Here v is the forward pelvis speed, $v^*=1.25$ m/s is the target speed, $N_m=26$ is the total number of muscles, $a_{j,t} \in [0, 1]$ is the activation of muscle j at timestep t with $a_{j,t-1}$ denoting the previous-step activation, \mathcal{J} is the set of tracked joints with per-joint imitation weights w_i , and $\rho = v^*/\dot{q}_{\text{pelvis}}^{\text{ref}}(t)$ scales the reference joint velocities to match the target walking speed. The control timestep is $\Delta t=0.02$ s and multiplying each term by Δt makes the reward magnitude independent of control frequency.

Stage 2 (Adaptation to Added Exoskeleton Mass). Stage 2 starts from the Stage 1 baseline human policy and attaches the exoskeleton structure to the musculoskeletal model. The pelvis-mounted frame and bilateral thigh links are parented directly to the corresponding human body segments, coupling the device mass and inertia into the body dynamics; assistance torques act coaxially at the human hip flexion joints, with passive abduction joints providing lateral compliance. In this stage, the exoskeleton actuator torque limit is set to zero in the simulation model, so no assistance torque is applied regardless of the actor output (Algorithm 1). The human policy continues training with the same reward in Eqs. (1) and (2). This stage isolates human adaptation to the added exoskeleton mass and inertia before active exoskeleton assistance is introduced.

Stage 3 (Learning of Assistance Timing with Frozen Human Policy). Stage 3 freezes the human policy and trains only the exoskeleton policy, using the stable Stage 2 walking pattern as a fixed environment for initial assistance timing learning. Hip imitation terms are disabled in this stage to prevent the exoskeleton from exploiting tracking rewards by resisting hip motion change rather than providing effective assistance to the hip flexor and extensor muscle groups.

A hip muscle activation term is added in Stage 3:

$$r_{\text{hip-act}} = -\Delta t \cdot \frac{1}{|\mathcal{M}_{\text{hip}}|} \sum_{m \in \mathcal{M}_{\text{hip}}} a_m^2, \quad (3)$$

Algorithm 1 Multi-stage Curriculum Training for Human-Exoskeleton Co-adaptation

- Require:** $v^* = 1.25$ m/s, $\Delta t = 0.02$ s (50 Hz), $\gamma = 0.99$
Ensure: Human policy π_h and exoskeleton policy π_e
- 1: Per-stage simulation steps: T_1, T_2, T_3, T_4
 - 2: Initialize π_h, π_e and shared critic V_ψ
 - 3: **Stage 1: Human baseline gait (imitation, human-only)**
 - 4: **for** $t = 1$ to T_1 **do**
 - 5: Roll out with π_h ; update (π_h, V_ψ) using PPO [13]
 - 6: **end for**
 - 7: Save $\pi_h^{(1)}$
 - 8: **Stage 2: Human adapts to a passive exoskeleton**
 - 9: Attach exoskeleton structure (mass/inertia added); load $\pi_h^{(1)}$; set exoskeleton torque to zero
 - 10: **for** $t = 1$ to T_2 **do**
 - 11: Roll out with π_h ; update (π_h, V_ψ) using PPO
 - 12: **end for**
 - 13: Save $\pi_h^{(2)}$
 - 14: **Stage 3: Exoskeleton pattern learning (human frozen)**
 - 15: Set $\tau_{\text{max}} \leftarrow 6$ Nm; freeze $\pi_h^{(2)}$; re-initialize π_e
 - 16: Disable hip imitation terms; add $r_{\text{hip-act}}$ (Eq. (3)) and $r_{\text{exo}}^{(3)}$ (Eq. (4))
 - 17: **for** $t = 1$ to T_3 **do**
 - 18: Roll out with frozen π_h and acting π_e ; update (π_e, V_ψ) using PPO
 - 19: **end for**
 - 20: Save $\pi_e^{(3)}$
 - 21: **Stage 4: Co-adaptation with power-based assistance**
 - 22: Set $\tau_{\text{max}} \leftarrow 25$ Nm; load $\pi_e^{(3)}$; unfreeze $\pi_h^{(2)}$
 - 23: Augment human observation with current exo torques $[\hat{u}_r, \hat{u}_l]$
 - 24: Expand human actor input by 2 dims; copy existing input weights; randomly initialize weights for the 2 new input dims
 - 25: Update $r_{\text{exo}}^{(4)}$ (Eq. (5)) and add $r_{\Delta\tau}$ (Eq. (6))
 - 26: **for** $t = 1$ to T_4 **do**
 - 27: Roll out with (π_h, π_e) ; update (π_h, π_e, V_ψ) using PPO
 - 28: **end for**
-

where $a_m \in [0, 1]$ is the activation of muscle m , and \mathcal{M}_{hip} includes iliopsoas, gluteus maximus, rectus femoris, and hamstrings on both legs.

In Stage 3, the exoskeleton torque limit is set to $\tau_{\text{max}} = 6$ Nm to constrain exploration during initial pattern learning and limit its perturbation to human control. The following reward is used to encourage positive assistance based on power sign and the use of higher assistance torques:

$$r_{\text{exo}}^{(3)} = \Delta t \sum_{j \in \{l, r\}} \alpha_d \hat{u}_j^2 \text{sign}(\hat{u}_j \omega_j), \quad (4)$$

where $\hat{u}_j \in [-1, 1]$ is the normalized torque command output by the exoskeleton actor and ω_j is the hip joint angular velocity. We set $\alpha_d = 0.5$. The Stage 3 exoskeleton policy is used to initialize Stage 4 joint training.

Stage 4 (Human-Exoskeleton Co-Adaptation).

Stage 4 starts the joint training of the human and exoskeleton policies for co-adaptation. The exoskeleton policy is loaded from Stage 3, the human policy is unfrozen, and the exoskeleton torque limit is set to the maximum motor torque $\tau_{\max} = 25$ Nm (Algorithm 1). The human actor observation is augmented with the current normalized exoskeleton torques $[\hat{u}_r, \hat{u}_l]$. In implementation, we expand the human actor input by two dimensions, keep the learned Stage 2 human actor weights for the original input dimensions, and randomly initialize the weights associated with the two new input dimensions. This keeps the learned walking policy while allowing the human actor to learn responses to exoskeleton torque during co-adaptation.

Both actors are trained jointly with a shared critic using the full system state. Stage 4 replaces the Stage 3 positive timing assistance reward ($r_{\text{exo}}^{(3)}$) with a power- and smoothness-based reward ($r_{\text{exo}}^{(4)}$), as the Stage 3 reward ($r_{\text{exo}}^{(3)}$) tends to produce saturated exoskeleton torques:

$$r_{\text{exo}}^{(4)} = \Delta t \sum_{j \in \{l, r\}} \left(\alpha \hat{u}_j \hat{\omega}_j - \beta \hat{u}_j^2 - \lambda_s \max(0, |\hat{u}_j| - \delta)^2 \right), \quad (5)$$

where $\hat{u}_j \in [-1, 1]$ is the normalized torque command and $\hat{\omega}_j = \text{clip}(\omega_j/\omega_s, -1, 1)$ is the normalized joint angular velocity (with $\omega_s = 2.0$ rad/s). The first term is related to mechanical power, rewarding torque that assists joint motion and penalizing torque that resists it. The second term penalizes torque magnitude to prevent the policy from preferring large torques. The third term adds a stronger penalty above the threshold δ , preventing actuator saturation when other reward terms drive torque upward. We set $\alpha = 0.3$, $\beta = 0.15$, $\lambda_s = 2.0$, and $\delta = 0.8$.

An exoskeleton torque-rate penalty is also added in Stage 4:

$$r_{\Delta\tau} = -\Delta t \sum_{j \in \{l, r\}} (\hat{u}_{j,t} - \hat{u}_{j,t-1})^2, \quad (6)$$

where $\hat{u}_{j,t}$ is the normalized torque command at time t . This term penalizes rapid torque changes for smooth assistance.

Stages 3 and 4 also include two auxiliary stability penalties: a joint constraint force penalty $r_{\text{constraint}} = -\Delta t \cdot \max_k (|f_k^{\text{joint}}|/mg)$, which penalizes joint limit forces normalized by body weight mg ; and a foot contact force penalty $r_{\text{foot}} = -\Delta t \cdot \max(0, (|f_r| + |f_l|)/mg - 1.2)$, which penalizes total foot contact forces exceeding 1.2 times body weight; both are inactive in Stages 1 and 2, where imitation rewards suffice to enforce stable gait. Stage 4 produces the final co-adapted policies; reward weights for all stages are listed in Table I.

The proposed four-stage training framework is modular: we keep the same architecture and simulation interface across stages and only change the training settings. Four dimensions are configurable: (i) *actor learning activation*: an actor can participate in rollout while its learning signal is disabled, so that only the other actor updates; (ii) *parameter freezing*: one actor’s weights can be fixed while the other updates, decoupling the two adaptation problems; (iii) *observation augmentation*: an actor’s input interface can be extended

TABLE II
PPO TRAINING HYPERPARAMETERS. VALUES ARE SHARED ACROSS STAGES UNLESS NOTED OTHERWISE.

Parameter	S1	S2–S4
Learning rate	5×10^{-5}	3×10^{-5}
PPO clip range	0.15	0.15
Rollout steps / env	2048	2048
Minibatch size	16384	16384
Epochs per update	20	20
Discount γ	0.99	0.99
GAE λ	0.95	0.95
Target KL	0.01	0.01
Max gradient norm	0.5	0.5
Entropy coefficient	0.001	0.001 / 0.003 ^a
Parallel environments	32	32

^a 0.003 for Stages 3 and 4.

TABLE III
HIP EXOSKELETON HARDWARE SPECIFICATIONS.

Item	Specification
Configuration	Custom-designed bilateral hip exoskeleton, Fig. 1.
Assistance plane	Sagittal plane (hip flex/ext)
Active DOF	1 per side (hip flexion and extension)
Passive DOF	1 per side (hip abd/add)
Actuator	MyActuator X8-25 BLDC (2 total)
Peak torque capacity	25 Nm per hip
Total mass	5.94 kg
Onboard computer	Raspberry Pi 4B
Controller input sensing	Built-in motor encoders
Command and logging rate	50 Hz and 50 Hz
Communication	CAN bus
Structure materials	Aluminum alloy, carbon tube, 3D printed parts using Nylon-Carbon fiber material (Onyx).

mid-training by appending new dimensions with existing weights preserved; and (iv) *reward activation*: stage-specific reward terms can be enabled or disabled per agent without modifying the network topology or the PPO update procedure [13]. The hyperparameters for the four-stage curriculum are listed in Table II. All training procedures were conducted on an Intel Xeon W-2145 (3.70 GHz, 8-core), achieving approximately 28 h per 100M simulation steps.

C. Hip Exoskeleton Hardware

A custom-designed bilateral hip exoskeleton was used to provide sagittal-plane hip assistance during treadmill walking (Fig. 1, right). Each side includes an actuated hip flexion and extension joint and a passive abduction and adduction joint, so the device can deliver assistance while accommodating subject fitting and natural lateral motion. For each subject, the exoskeleton hip joint axis was aligned with the anatomical hip joint axis during device fitting.

The exoskeleton control policy obtained from Stage 4 was deployed on a Raspberry Pi 4B mounted on the exoskeleton frame, communicating with the MyActuator X8-25 motors via CAN bus at 50 Hz. The deployed policy receives joint-state information from the exoskeleton motor encoders and outputs a normalized torque command within $[-1, 1]$. This command is then scaled by the preset per-hip torque limit

used in the experiment to generate the commanded hip torque.

During treadmill walking, standard safety protections were applied, including access to an emergency stop, software torque limit, and operator supervision. Hardware specifications of the device are summarized in Table III.

D. Experimental Design

Five participants with no mobility impairment enrolled in the treadmill walking experiment under IRB approval with informed consent. Each subject wore the hip exoskeleton and completed a fixed-order protocol: a 5 min familiarization trial, a 5 min no-assist trial (exoskeleton worn, commanded torque set to zero with back-drivable hip actuators), and two 5 min assist trials at 10 Nm and 15 Nm torque limits, with a 2 min rest between all conditions. All trials were performed at 1.25 m/s (2.8 mph) on a treadmill.

We conducted analyses of bilateral hip joint angle, angular velocity, and commanded torque, along with assistance mechanical power $P_{\text{command}} = \tau_{\text{command}}\omega$. Angular velocity was filtered with a One Euro filter before power calculation [14], and gait cycles were segmented using peak hip flexion as the reference event.

E. Exoskeleton Torque and Power Analysis

To quantify the mechanical output of the exoskeleton controller, four metrics were computed per subject and condition following [15]: root-mean-square torque (τ_{RMS} , Nm), mean peak torque (τ_{MAX} , Nm), mean positive power (MPP, W), and mean negative power (MNP, W). Gait cycles were segmented at peak hip flexion, used as the reference event in the absence of ground-reaction force sensors. For each cycle, MPP and MNP were computed as

$$\text{MPP} = \frac{1}{n} \sum_{\tau_i \dot{q}_i > 0} \tau_i \dot{q}_i, \quad \text{MNP} = \frac{1}{n} \sum_{\tau_i \dot{q}_i < 0} \tau_i \dot{q}_i, \quad (7)$$

where τ_i and \dot{q}_i are the filtered hip joint torque and angular velocity, and n is the total number of samples per cycle. All metrics were averaged across gait cycles per subject.

III. RESULTS

A. Simulation Evaluation of Stable Walking and Effects of Assistance

Stage 1 trains the human musculoskeletal actor without any exoskeleton, converging over approximately 320 M simulation steps (Fig. 2). The learned gait shows strong bilateral symmetry across all joints (Pearson $r > 0.92$), with toe-off at $57.8 \pm 1.1\%$ (right) and $58.5 \pm 0.9\%$ (left) of the gait cycle, consistent with physiological norms for treadmill walking [16]. In Stage 2, the exoskeleton structure is attached with its torque output set to zero, and the human actor is fine-tuned to accommodate the added device mass and inertia. Starting from the Stage 1 policy, convergence is reached within approximately 160 M steps (Fig. 2), roughly half the steps required in Stage 1. Joint trajectories are well preserved (RMSE $< 3.6^\circ$ for all joints; Pearson $r > 0.92$

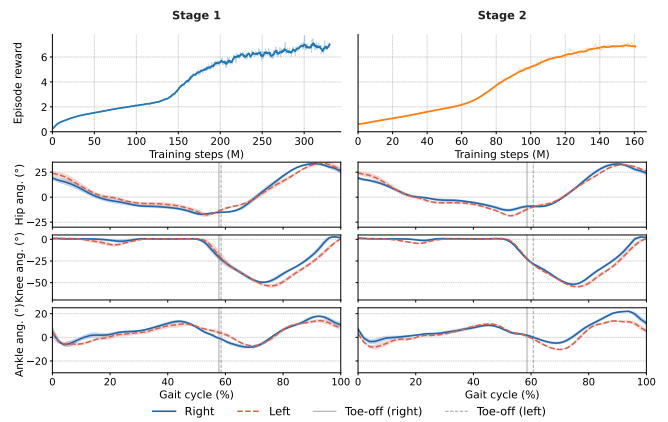


Fig. 2. Training reward curves and joint kinematics for Stages 1 and 2 (left and right columns, respectively). **Top:** Episode reward over training steps. **Bottom:** Mean ± 1 s.d. hip, knee, and ankle angle trajectories over the normalized gait cycle; right limb (solid blue), left limb (dashed red). Vertical lines: mean toe-off.

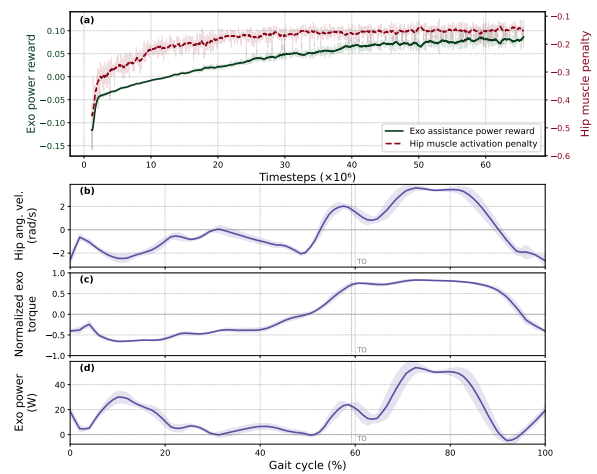


Fig. 3. Stage 4 co-adapted profiles. **(a)** Exoskeleton assistance power reward (left axis, green) and hip muscle activation penalty (right axis, red dashed) over training. **(b)** Hip angular velocity over the gait cycle (positive: flexion; negative: extension). **(c)** Normalized exoskeleton torque. **(d)** Exoskeleton mechanical power. Panels (b–d): bilateral average; shaded region: ± 1 SD. Dotted vertical line: mean toe-off.

across all joint pairs), and bilateral symmetry is maintained throughout [17].

Stage 3 establishes an initial flexion-assist timing pattern in approximately 1.1 M simulation steps; Stage 4 refines this through full co-adaptation over approximately 66 M steps. As shown in Fig. 3a, the exoskeleton assistance power reward increases from -0.12 to 0.08 and the hip muscle activation penalty decreases in magnitude over the course of training. The final co-adapted torque profile (Fig. 3c), plotted alongside the hip angular velocity (Fig. 3b), indicates that the exoskeleton torque is predominantly aligned with joint motion throughout the gait cycle, with peak normalized torque of 0.83 occurring at 75% of the gait cycle during the late-swing flexion phase, reducing the negative-work time fraction (fraction of the gait cycle where $P = \tau\dot{q} < 0$) to 10% , as reflected in Fig. 3d.

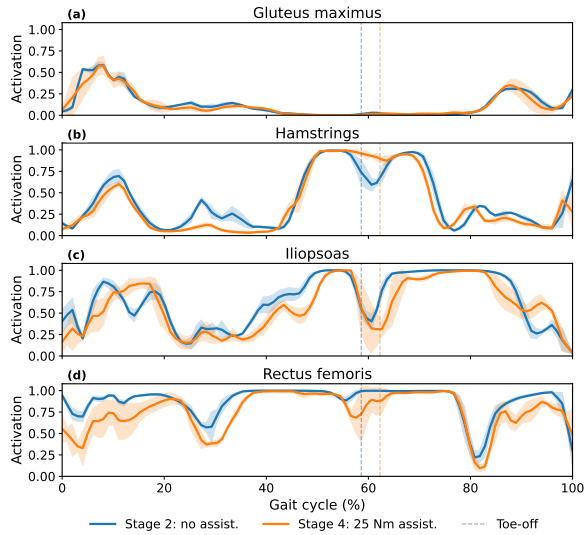


Fig. 4. Right-side hip muscle activation over the gait cycle comparing Stage 2 (no assistive torque, blue) and Stage 4 (maximum assistive torque 25 Nm, orange). Shaded bands: mean \pm 1 s.d. Dashed vertical lines mark mean toe-off for each condition.

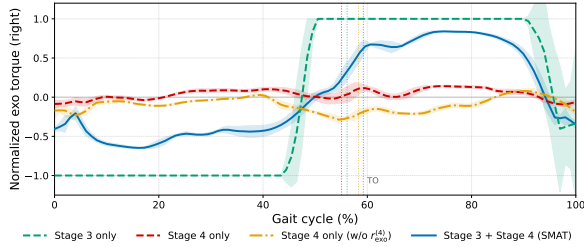


Fig. 5. Ablation comparing right-hip normalized exo torque over the gait cycle under four conditions: **Stage 3 only** without Stage 4 co-adaptation (dashed green); **Stage 4 only** initialized from Stage 2 without Stage 3 pre-training (dashed red, mean across three runs); **Stage 4 only without** $r_{\text{exo}}^{(4)}$, initialized from Stage 2 (dash-dot orange); and the full **Stage 3 + Stage 4 (SMAT)** pipeline (solid blue). Dotted vertical lines mark mean toe-off.

The reduction in hip muscle activation is further quantified in Fig. 4, comparing right-side activation between Stage 2 (no assistive torque) and Stage 4 (maximum assistive torque, $\tau_{\text{max}} = 25$ Nm). All four muscles show reduced mean activation with exoskeleton assistance, averaging 10.1% across muscles. The largest reductions are in the primary hip flexors: rectus femoris (-13.5%) and iliopsoas (-10.5%), whose swing-phase activation is partially substituted by the exoskeleton’s flexion torque. Hamstrings decrease by 9.7% and gluteus maximus by 6.6%, with the smaller extensor reductions consistent with the learned torque profile providing less direct offloading during stance.

Ablation: necessity of Stage 3 and Stage 4. As shown in Fig. 5, three ablation conditions reveal the necessity of both stages. Without Stage 4 co-adaptation (Stage 3 only), the torque saturates at $\pm \hat{\tau}_{\text{max}}$ for most of the gait cycle and reverses abruptly near toe-off, imposing impulsive hip loading that would pose safety concerns in physical human–robot interaction [18]. Without Stage 3 pre-training (**Stage 4 only**), training collapses to a local optimum: the second

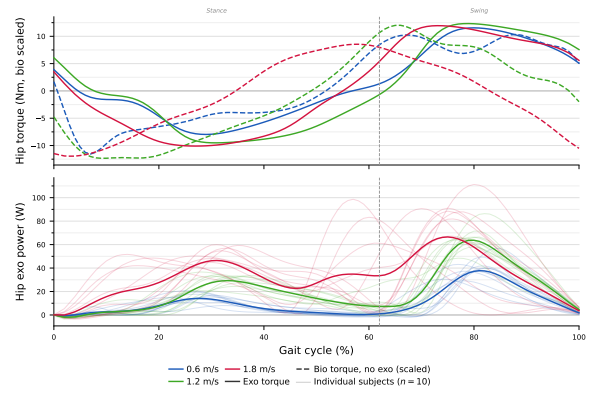


Fig. 6. Speed generalization on the GT dataset [19] (10 subjects, 0.6, 1.2, and 1.8 m/s; blue/green/red). *Top*: Gait-cycle-normalized group mean hip torque; solid: exo torque, dashed: biological hip torque (no-exo condition, amplitude scaled for timing comparison). *Bottom*: Hip exo power; thin lines: individual subjects, bold: group mean. Dashed vertical line: toe-off ($\approx 62\%$).

term of (5) rewards minimising torque magnitude, so the policy discovers that producing no torque maximises that reward component, yielding near-zero output (peak normalized torque 0.14 vs. 0.84, an 83% reduction), with 32% of this minimal torque opposing joint motion (vs. 10% in the full SMAT pipeline). Removing $r_{\text{exo}}^{(4)}$ entirely (**Stage 4 only w/o** $r_{\text{exo}}^{(4)}$) causes the exoskeleton to converge to a slight constant extension torque, which persistently opposes hip flexion during swing and results in negative exo power for 40% of the gait cycle. These three conditions confirm that both Stage 3 pre-training and Stage 4 co-adaptation are required components of the full SMAT pipeline.

B. Verification of Assistance Efficiency and Speed Generalization with Open Source Dataset

To evaluate generalizability beyond training conditions, we assessed the SMAT-trained exo actor on an open source dataset [19], comprising 10 subjects walking at 0.6, 1.2, and 1.8 m/s. Importantly, the policy receives only hip kinematics as input, enabling potential generalization to different walking speeds without the need for explicit speed-based adjustment.

Fig. 6 shows gait-cycle-normalized exo torque profiles alongside the biological hip torque (amplitude scaled to match exo peak for timing comparison). Peak assistive torque remained consistent across all speeds (11.6–12.3 Nm), well within the 15 Nm chosen maximum. The exo torque profile lagged biological hip torque by 9–20% of the gait cycle (~ 156 – 210 ms, by cross-correlation of torque waveforms) across all three speeds. In the work by Molinaro et al. [19], the authors intentionally imposed a 125 ms hip-assistance delay to maximize positive mechanical work. Our policy produces a similar phase offset through reward optimization alone, without explicit timing constraints [20]. Peak exo power reached 38–67 W in early-to-mid swing, consistent with the biological assistive demand, and timing remained stable across all speeds and subjects without subject-specific retraining.

TABLE IV
PER-SUBJECT EXOSKELETON JOINT TORQUE AND POWER METRICS ACROSS ASSISTANCE CONDITIONS

Subject No.	10 Nm				15 Nm			
	τ_{RMS} (Nm)	τ_{MAX} (Nm)	MPP (W)	MNP (W)	τ_{RMS} (Nm)	τ_{MAX} (Nm)	MPP (W)	MNP (W)
S1	6.12	8.12	14.93	-0.16	9.40	12.25	26.58	-0.14
S2	6.13	8.14	17.26	-0.11	9.67	12.13	29.91	-0.10
S3	5.87	8.07	11.74	-0.15	9.07	12.39	20.02	-0.18
S4	5.89	7.95	12.90	-0.09	9.13	12.03	22.01	-0.18
S5	5.97	8.02	11.27	-0.10	9.14	12.30	20.51	-0.10
Mean (\pm SD)	6.0 ± 0.1	8.1 ± 0.1	13.6 ± 2.5	-0.1 ± 0.0	9.3 ± 0.3	12.2 ± 0.1	23.8 ± 4.3	-0.1 ± 0.0

τ_{RMS} : root-mean-square torque; τ_{MAX} : mean peak torque; MPP: mean positive power; MNP: mean negative power. Gait cycles segmented at peak hip flexion angle. All metrics computed for the right leg.

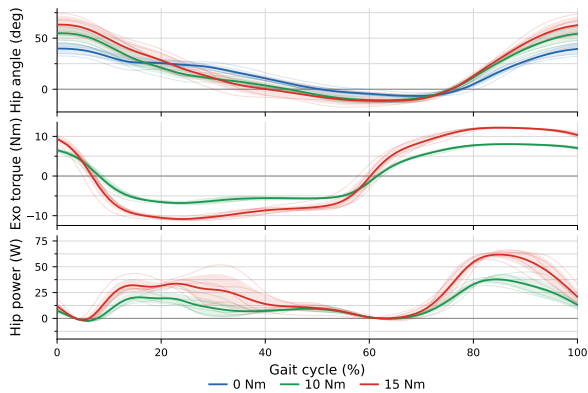


Fig. 7. Hip kinematics, exo torque, and mechanical power under assisted conditions (0% = peak hip flexion; 0Nm: blue, 10Nm: green, 15Nm: red). **Top:** Group-mean right hip angle. **Middle:** Exoskeleton torque. **Bottom:** Right hip assistance power. Shaded bands: ± 1 SD; thin lines: subject means.

C. Validation with Human Experiment

We evaluated the sim-to-real transfer of the SMAT-trained policy on five healthy participants (S1–S5) across three assistance levels: 0Nm, 10Nm, and 15Nm. Fig. 7 and Table IV summarize the measured hip kinematics and joint-level mechanical output.

Hip kinematics. As shown in Fig. 7 (top), the waveform shape remained consistent across conditions: peak hip extension occurred in late stance (≈ 62 – 68% gait cycle) and hip flexion accelerated into swing phase, matching the normal gait pattern. These results confirm that the controller modulates assistance without altering gait timing.

Joint work analysis. All metrics are reported for the right leg. Fig. 7 (middle) shows that the exo torque waveform is consistent across subjects, with a positive assistive peak in mid-swing; peak torque scales with the commanded level (8.1 ± 0.1 Nm at 10 Nm limit, 12.2 ± 0.1 Nm at 15 Nm limit). As shown in Fig. 7 (bottom) and reported in Table IV, MPP increased from 13.6 ± 2.5 W at 10Nm to 23.8 ± 4.3 W at 15Nm, confirming that the policy scales mechanical energy delivery in proportion to the commanded assistance level, while MNP remained very small (≈ -0.1 W) in both conditions, indicating low resistive losses. Subject consistency confirms that the policy delivers assistance at the correct timing without subject-specific parameter adjustment. At a comparable τ_{RMS} of approximately 6 Nm, the delayed output

feedback controller of Lim et al. [21] reported an MPP of 9.9–11.6 W during treadmill walking at 4 km/h, while our policy achieved 13.6 W at the same RMS torque, indicating more efficient positive-power delivery per unit RMS torque.

IV. DISCUSSION

The ablation study clarifies the functional role of Stages 3 and 4 and demonstrates that both are necessary for stable co-adaptation. When Stage 3 is removed and Stage 4 begins from a randomly initialized exoskeleton policy, training consistently converges to a near-zero torque solution, regardless of whether Stage 4 includes $r_{\text{exo}}^{(4)}$ or not. In this setting, the exoskeleton minimizes disturbance to the imitation and muscle penalties by outputting negligible torque. This represents a local optimum in which assistance is avoided rather than learned. Stage 3 prevents this collapse by isolating assistance timing learning under controlled conditions. Freezing the human policy removes non-stationarity, while the reduced torque limit ($\tau_{\text{max}} = 6$ Nm) constrains destabilizing exploration. The additional reward $r_{\text{exo}}^{(3)}$ explicitly encourages torque aligned with joint velocity, establishing a positive mechanical power pattern before full co-adaptation. This warm-start ensures that Stage 4 begins from a meaningful assistance strategy rather than from zero-output behavior.

From a sim-to-real perspective, sensing modality introduces practical limitations. In simulation, hip angles correspond to anatomical joint motion, whereas on hardware the policy relies on exoskeleton encoder measurements. Due to soft tissue compliance and strap looseness at the thigh cuffs and waist belt, encoder-derived angles may overestimate true biological hip motion. Velocity estimates are also noisier than motion-capture signals used in offline evaluation, particularly during gait transitions. This kinematic mismatch can degrade timing precision in physical deployment. Replacing encoder-based estimates with thigh- and pelvis-mounted IMUs could provide more accurate biological hip kinematics and smoother velocity signals [22], improving phase estimation and assistance alignment.

The learned controller operates below the torque limit. This behavior is shaped by the Stage 4 saturation penalty (Eq. (5), $\delta = 0.8$), which discourages impulsive loading, eliminates high-amplitude torque bursts, and prevents resistive extension strategies that push the negative-work fraction higher. We also observed mild inter-limb asymmetry in hip angular velocity, likely due to the absence of an explicit

symmetry constraint during training. Incorporating a bilateral symmetry term could further regularize assistance profiles.

In simulation, hip muscle activation decreased by 10.1% on average. However, physiological validation remains necessary. Real users may redistribute effort across muscle groups or gradually alter coordination patterns as adaptation progresses. Future studies incorporating EMG and indirect calorimetry [23], [24] will determine whether simulated offloading translates to measurable metabolic benefit. The current human evaluation included five healthy participants at a single treadmill speed. Broader validation across larger cohorts, varied walking speeds, and clinical populations will better characterize generalization [25].

V. CONCLUSIONS

Co-adaptive exoskeleton control is challenging because jointly training human and exoskeleton policies creates a non-stationary learning problem prone to instability or poor local optima. SMAT addresses this with four sequential stages separating gait learning, passive adaptation, assistance-timing pre-training, and full co-adaptation. The ablation study confirms each stage is necessary for stable co-adaptation. The final trained controller reduced hip muscle activation by 10.1% in simulation, generalized to unseen subjects across 0.6–1.8 m/s without explicit speed adjustment, and transferred to hardware without subject-specific retraining. The deployed controller delivered consistent assistance timing and predominantly positive mechanical power (MPP: 13.6–23.8 W, with negative power below 1.3% of MPP) across five participants. Compared with prior hip-exoskeleton controllers, the proposed controller achieves more effective positive-power delivery per unit RMS torque, indicating improved assistance efficiency. Notably, the policy yields an emergent assistance-phase delay of 9–20% of the gait cycle that mirrors biomechanically optimal hip-assistance phasing [19]. Future work will validate simulated muscle offloading via EMG and indirect calorimetry.

REFERENCES

- [1] A. Rodríguez-Fernández, J. Lobo-Prat, and J. M. Font-Llagunes, “Systematic review on wearable lower-limb exoskeletons for gait training in neuromuscular impairments,” *Journal of neuroengineering and rehabilitation*, vol. 18, no. 1, p. 22, 2021.
- [2] R. Baud, A. R. Manzoori, A. Ijspeert, and M. Bouri, “Review of control strategies for lower-limb exoskeletons to assist gait,” *Journal of neuroengineering and rehabilitation*, vol. 18, no. 1, p. 119, 2021.
- [3] K. L. Poggensee and S. H. Collins, “How adaptation, training, and customization contribute to benefits from exoskeleton assistance,” *Science Robotics*, vol. 6, no. 58, p. eabf1078, 2021.
- [4] S. Luo, G. Androwis, S. Adamovich, E. Nunez, H. Su, and X. Zhou, “Robust walking control of a lower limb rehabilitation exoskeleton coupled with a musculoskeletal model via deep reinforcement learning,” *Journal of neuroengineering and rehabilitation*, vol. 20, no. 1, p. 34, 2023.
- [5] S. Luo, M. Jiang, S. Zhang, J. Zhu, S. Yu, I. Dominguez Silva, T. Wang, E. Rouse, B. Zhou, H. Yuk *et al.*, “Experiment-free exoskeleton assistance via learning in simulation,” *Nature*, vol. 630, no. 8016, pp. 353–359, 2024.
- [6] G. Leem, J. Lee, J. Lee, S. Song, and J. Won, “Exo-plore: Exploring exoskeleton control space through human-aligned simulation,” *arXiv preprint arXiv:2601.22550*, 2026.
- [7] Y. Yuan, G. Androwis, and X. Zhou, “Gait asymmetry from unilateral weakness and improvement with ankle assistance: a reinforcement learning based simulation study,” *arXiv preprint arXiv:2602.18862*, 2026.
- [8] N. Ratnakumar, M. H. Tohfafarosh, S. Jauhri, and X. Zhou, “Reinforcement-learning-based assistance reduces squat effort with a modular hip–knee exoskeleton,” *arXiv preprint arXiv:2602.17794*, 2026.
- [9] Y. Bengio, J. Louradour, R. Collobert, and J. Weston, “Curriculum learning,” in *Proceedings of the 26th annual international conference on machine learning*, 2009, pp. 41–48.
- [10] A. S. Chiappa, P. Tano, N. Patel, A. Ingster, A. Pouget, and A. Mathis, “Acquiring musculoskeletal skills with curriculum-based reinforcement learning,” *Neuron*, vol. 112, no. 23, pp. 3969–3983, 2024.
- [11] V. Caggiano, H. Wang, G. Durandau, M. Sartori, and V. Kumar, “Myosuite—a contact-rich simulation suite for musculoskeletal motor control,” *arXiv preprint arXiv:2205.13600*, 2022.
- [12] C. K. Tan, C. Wang, S. Lyu, B. K. Hodossy, P. Schumacher, E. B. Wilson, V. Caggiano, V. Kumar, D. Farina, L. Gionfrida *et al.*, “Myoassist 0.1: Myosuite for dexterity and agility in bionic humans,” in *2025 International Conference On Rehabilitation Robotics (ICORR)*. IEEE, 2025, pp. 437–442.
- [13] J. Schulman, F. Wolski, P. Dhariwal, A. Radford, and O. Klimov, “Proximal policy optimization algorithms,” *arXiv preprint arXiv:1707.06347*, 2017.
- [14] G. Casiez, N. Roussel, and D. Vogel, “1€ filter: a simple speed-based low-pass filter for noisy input in interactive systems,” in *Proceedings of the SIGCHI Conference on human factors in computing systems*, 2012, pp. 2527–2530.
- [15] B. Lim, B. Choi, C. Roh, S. Hyung, Y.-J. Kim, and Y. Lee, “Parametric delayed output feedback control for versatile human-exoskeleton interactions during walking and running,” *IEEE Robotics and Automation Letters*, vol. 8, no. 8, pp. 4497–4504, 2023.
- [16] J. Perry and J. Burnfield, *Gait analysis: normal and pathological function*. CRC Press, 2024.
- [17] W. Forczek and R. Staszkiwicz, “An evaluation of symmetry in the lower limb joints during the able-bodied gait of women and men,” *Journal of human kinetics*, vol. 35, p. 47, 2012.
- [18] J. C. Moreno, F. Brunetti, E. Navarro, A. Former-Cordero, and J. L. Pons, “Analysis of the human interaction with a wearable lower-limb exoskeleton,” *Applied Bionics and Biomechanics*, vol. 6, no. 2, pp. 245–256, 2009.
- [19] D. D. Molinaro, K. L. Scherpereel, E. B. Schonhaut, G. Evangelopoulos, M. K. Shepherd, and A. J. Young, “Task-agnostic exoskeleton control via biological joint moment estimation,” *Nature*, vol. 635, no. 8038, pp. 337–344, 2024.
- [20] I. Kang, P. Kunapuli, and A. J. Young, “Real-time neural network-based gait phase estimation using a robotic hip exoskeleton,” *IEEE Transactions on Medical Robotics and Bionics*, vol. 2, no. 1, pp. 28–37, 2019.
- [21] B. Lim, J. Lee, J. Jang, K. Kim, Y. J. Park, K. Seo, and Y. Shim, “Delayed output feedback control for gait assistance with a robotic hip exoskeleton,” *IEEE Transactions on Robotics*, vol. 35, no. 4, pp. 1055–1062, 2019.
- [22] T. Seel, J. Raisch, and T. Schauer, “Imu-based joint angle measurement for gait analysis,” *Sensors*, vol. 14, no. 4, pp. 6891–6909, 2014.
- [23] F. Sylos-Labini, V. La Scaleia, A. d’Avella, I. Pisotta, F. Tamburella, G. Scivoletto, M. Molinari, S. Wang, L. Wang, E. Van Asseldonk *et al.*, “Emg patterns during assisted walking in the exoskeleton,” *Frontiers in human neuroscience*, vol. 8, p. 423, 2014.
- [24] K. Seo, J. Lee, Y. Lee, T. Ha, and Y. Shim, “Fully autonomous hip exoskeleton saves metabolic cost of walking,” in *2016 IEEE International Conference on Robotics and Automation (ICRA)*. IEEE, 2016, pp. 4628–4635.
- [25] Y. Chen, S. Miao, G. Chen, J. Ye, C. Fu, B. Liang, S. Song, and X. Li, “Learning to assist different wearers in multitasks: efficient and individualized human-in-the-loop adaptation framework for lower-limb exoskeleton,” *IEEE Transactions on Robotics*, vol. 40, pp. 4699–4718, 2024.